Available online at www.sciencedirect.com
ScienceDirect
Journal of Magnetic Resonance 183 (2006) 134–141
JMR Journal of Magnetic Resonance
www.elsevier.com/locate/jmr

Ultra-low field NMR measurements of liquids and gases with short relaxation times

P.L. Volegov, A.N. Matlachov, R.H. Kraus Jr. *

Los Alamos National Laboratory, Biological and Quantum Physics Group, Los Alamos, NM 87545, USA

Received 26 April 2006; revised 18 July 2006
Available online 1 September 2006

Abstract

Interest in nuclear magnetic resonance measurements at ultra-low magnetic fields (ULF, ~μT fields) has been motivated by various benefits and novel applications including narrow NMR peak-width, negligible susceptibility artifacts, imaging of samples inside metal containers, and possibility of directly imaging neuronal currents. ULF NMR/MRI is also compatible with simultaneous measurements of biomagnetic signals. However the most widely used technique in ULF NMR—prepolarization at high field and measurement at lower field—results in large transient signals which distort the free induction decay signal. This is especially severe for the measurement of signals from samples and materials with short T_1 time. We have devised an approach that largely cancels the transient signals. The technique was successfully used to measure NMR signals from liquids and gases with T_1 in the range 1–4 ms.

Keywords: Ultra-low field; NMR; Microtesla; Transient; Noise; Fast relaxation

1. Introduction

There has been increasing interest and progress in ultra-low field (ULF, ~μT fields) NMR and MRI in recent years. Conventional approaches to magnetic resonance imaging (MRI) have strived for ever greater magnetic field strengths [1]. Higher magnetic fields (commonly 3–10 T or more) are sought to improve signal-to-noise by increasing sample polarization and Larmor frequencies (ω_L). Greater imaging fields also increase resolution by decreasing the voxel size required to obtain a given signal-to-noise. In contrast, ULF MRI has been motivated by a variety of potential benefits such as smaller magnetic field induced artifacts, narrow NMR line widths, simultaneous detection of multiple nuclei, and the prospect of systems with reduced cost and size [2]. Important medical motivators include the desire to avoid complications caused by high field (HF) MRI of subjects containing metal (i.e., metal pins or implants), that would be essentially eliminated at low fields. Not only can samples containing metal be imaged at ULF, we have also demonstrated that samples entirely contained within metallic containers can be imaged at ULF [3]. The ability to measure NMR signals through metal enables noninvasive detection of contraband or monitoring of flow and mass transport in chemical processes.

Magnetic resonance imaging at ULF also offers other advantages. For a fixed relative inhomogeneity, broadening of the NMR line scales linearly with the strength of the measurement field providing very narrow NMR lines (limited by the natural linewidth) with high signal-to-noise, enabling MRI at lower gradients [4]. Susceptibility artifacts caused by coupling between the applied magnetic field and varying susceptibility within the sample, broaden resonance lines at HF but are negligible at ULF. The absence of such artifacts should provide opportunities for novel forms of static and functional imaging at ULF such as the possibility of manipulating T_1 contrast to provide significant contrast not always realized at HF [5]. All of these effects combine to offer the prospect that MRI at low fields may provide a regime of high sensitivity and resolution, with unique applications.

* Corresponding author. Fax: +1 505 665 4507.
E-mail address: rkraus@lanl.gov (R.H. Kraus Jr.).

1090-7807/$ - see front matter © 2006 Elsevier Inc. All rights reserved.
doi:10.1016/j.jmr.2006.07.021

NMR and MRI detect the magnetic signature of nuclear spins processing in the measurement magnetic field at the characteristic ω_L. The difficulty of detecting NMR/MRI signals at ULF is primarily due to the decreased spin polarization. The superconducting quantum interference device (SQUID) is a magnetic flux-to-voltage converter of exquisite sensitivity with a response that is independent of frequency (hence, the sensitivity is independent of ω_L). Consequently, a growing number of low-field NMR/MRI systems have employed SQUID sensors (e.g., [3,4,6–11]). The frequency independent response of SQUID detectors readily enables one to simultaneously detect the signatures from multiple nuclei, even when their NMR frequencies may differ by factors of two or more [12].

The small signal amplitude of the ULF NMR signal caused by low polarization ratios is largely offset by pre-polarizing the sample at fields significantly larger than the measurement field and the extraordinary sensitivity of the SQUID sensors. Switching the pre-polarizing field results in large transients that distort the free induction decay (FID) NMR signal. Distortion of the FID degrades all NMR measurements and eddy-current transients are particularly problematic for materials with short relaxation times because there may be no residual signal after the transient effects decay away. In this paper we describe an approach to largely cancel the transient signals and their effect on the FID measurement. We focus on materials with short relaxation times because the effect is most evident in this regime for the simplest pulse sequences (as described below). The technique is nonetheless important for all relaxation times, especially when pulse sequences (such as echo or gradient pulses) are used during the signal acquisition.

2. Method

The most widely used NMR/MRI technique for low fields consists of polarizing the sample in a large field B_p, then, switching off B_p in a time short compared to T_1 and observing the free induction decay (FID) of the magnetization of the sample at a low field B_m. If the polarization field is switched off adiabatically ($\mathrm{d}B/\mathrm{d}t \ll \gamma B^2$) the bulk magnetization becomes aligned along the measurement field B_m and it is then necessary to apply a $\pi/2$ pulse to observe the precession of the magnetization. Alternatively, if B_p is switched off non-adiabatically ($\mathrm{d}B_p/\mathrm{d}t \geqslant \gamma B_m^2$) then the magnetization remains aligned along B_p and, if B_m is not parallel to B_p, the precession of the bulk magnetization is directly observable [13]. In practice B_p is switched off in two stages: first it is reduced adiabatically to some intermediate value, B_p', still significantly larger than the measurement field, after which the remaining field decreases non-adiabatically in a time that is short compared with $(\gamma B_p')^{-1}$ [13–15]. However the total time to decrease B_p below B_m should be short relative to the T_1 of the sample.

Rapidly switching off B_p inevitably results in the transient field which arises from the currents proportional to $\mathrm{d}B/\mathrm{d}t$ induced in any conductive materials (e.g., other components of the experimental apparatus and surrounding equipment). The two stage switching of B_p significantly reduces the magnitude of the observed transients for samples with moderately long T_1 times (tens of milliseconds). However, for samples with T_1 times on the order of a few milliseconds it is necessary to switch B_p off in a matter of a millisecond or less resulting in large unavoidable transients.

For example, a typical ULF NMR protocol we have used [16], pre-polarizes a sample at $B_p \sim 20$ mT, then non-adiabatically reduces B_p within 0.35 ms, resulting in large transient-induced signals measured by the SQUID sensors. We have carefully optimized our system to minimize these transients; however they remain as large as 0.1 μT in amplitude and ~10–20 ms in duration. While the transient fields are significantly smaller than B_m (~1–10 μT), hence they do not significantly alter the evolution of the spins, they are much larger than the typical signal from bulk magnetization of the sample (~1 pT or 10^{-12} T) thus impeding or even preventing measurement of the NMR signal and the associated NMR parameters.

To illustrate this in detail we write the measured signal as follows:

$$S(t) = F(t) + T(t) + \xi(t),$$

where: $S(t)$ is the measured signal, $F(t)$ is the free induction decay signal, $T(t)$ is the transients, and ξ(t) is the noise signal. ξ(t) is usually assumed to be uncorrelated with the measurements, hence averaging repeated measurements effectively reduces the noise. In contrast, the transient signals *are* synchronized with the measurements and can not be removed or reduced by averaging.

One approach to correct for the transient signals is to approximate the transients and subtract them in post processing. One can estimate $T(t)$ with a sum of exponents (typically 2–3)

$$\tilde{T}(t) = a + \sum_{i=1}^{n} b_i \mathrm{e}^{-\lambda_i t}, \tag{1}$$

where the approximation parameters $\{a, b_i, \lambda_i\}_1^n$ are fit by minimizing the difference between the measured signal $S(t)$ and the transients approximation

$$\{a, b_i, \lambda_i\}_1^n : \min_{\{a,b_i,\lambda_i>0\}_1^n} \|S(t) - \tilde{T}(t)\|.$$

The estimate of the FID is then given by: $\tilde{F}(t) = S(t) - \tilde{T}(t)$—will then be largely free of the transient-induced signals resulting in a much smaller overall dynamic range and additional digital filters can be farther applied to enhance the FID with only minimal filtering artifacts.

We have previously used this approach with good success [3,12,17], however we have recognized some inherent drawbacks. First, while approximating the transient signal with a few exponentials works relatively well, it is only effective ~10 ms after the B_p cut-off time. Hence, for sam-

ples with short T_1 times (<10 ms) this approximation is not adequate. The second drawback is apparent when the measured signal contains other low frequency signals (e.g., MEG signal in simultaneous MEG/NMR measurements [17]), to which digital filtering cannot be applied without distorting the desired signals.

We have devised a new approach that does not have the drawbacks discussed above while removing the transients even more effectively and potentially removing other correlated noise sources as well. Our new technique largely cancels transient-induced signals by acquiring interleaved NMR measurements at two different measurement fields (i.e., two different ω_L) and differencing these two signals. We write the measured signal as

$$S_k(t) = F_k(t) + T(t) + \xi_k(t), k = \overline{1,2n},$$

where the subscript k numerates the measurements. The total number of the measurements is $2n$, where n is the number of the measurements with one frequency. We assume that the transient-induced signal does not depend on the amplitude of the measurement field, thus it is the same in all measurements. The FID signal for each measurement can be expressed using Fourier transform of the "normal" measurements as

$$F_k(t) = \int F_0(\omega') e^{i(\omega' + (\omega_k - \omega_0))t} d\omega',$$

$$\omega_k = \begin{cases} \omega_0, & k - \text{odd}, \\ \omega_0 - \Delta\omega, & k - \text{even}. \end{cases}$$

The estimation of the FID signal is the mean difference between odd and even measurements

$$\begin{aligned} \tilde{F}(t) &= \frac{1}{n}\sum_{k=0}^{n-1}(S_{2k+1} - S_{2k}) \\ &= \frac{1}{n}\sum_{k=1,3\ldots}^{2n-1} S_k(t) - \frac{1}{n}\sum_{k=2,4\ldots}^{2n} S_k(t) \\ &= \int F_0(\omega') e^{i\omega' t}(1 - e^{-i\Delta\omega t})\, d\omega'. \end{aligned} \tag{2a}$$

Or in the frequency domain

$$\tilde{F}(\omega) = F_0(\omega) - F_0(\omega + \Delta\omega) \tag{2b}$$

The noise, ξ(t), is omitted from Eqs. (2a) and (2b) and subsequent discussion because it is assumed to be removed by averaging. Using this approach the transient-induced portion of the measured signal will be largely removed from the resulting signal, while the NMR signals will be retained if the frequency shift is non zero (forced by measuring at two ω_L).

We assume that the NMR signals consist of a finite number of damped harmonic components

$$F_0(t) = \sum_{k=1}^{m} A_k e^{(-\alpha_k + i\omega_k)t}, \tag{3}$$

where m is the number of harmonic components, i.e., the number of NMR peaks in the original spectrum.

The NMR signal parameters, $\{A_k, \alpha_k, \omega_k\}_1^m$ can be estimated using, for example, the direct exponential curve resolution algorithm (DECRA) [18]. The DECRA method constructs a Hankel matrix from a single FID which is partitioned into two submatrices and then the decay constants and the individual signals in the FID are recovered by solving a generalized eigenvalue-eigenvector problem for these matrices. For our two-frequency approach, we will obtain twice the number of components: $\{A_k, \alpha_k, \omega_k\}_1^m$ and $\{\tilde{A}_k, \tilde{\alpha}_k, \tilde{\omega}_k\}_1^m$ which should satisfy to the following condition:

$$A_k = -\tilde{A}_k, \quad \alpha_k = \tilde{\alpha}_k, \quad \omega_k - \tilde{\omega}_k = \Delta\omega, \quad k = \overline{1,m}. \tag{4}$$

This last condition can be used as a consistency check to validate the estimation of the FID parameters or can be used as an *a priori* condition in various maximum likelihood techniques for estimating parameters of the NMR signal either in time (discrete exponential fitting) or in frequency (Lorentzian fitting) domains [19,20].

We note that in the limiting case $\Delta\omega = \omega_0$, i.e., the second measurement is performed with zero measurement field, the estimation of the FID according to the Eq. (2a) directly gives the "typical" single-frequency FID. Practical considerations, however, dictate that to most efficiently reduce transient-induced and other correlated signal noise, ΔB_m (and hence $\Delta\omega$) should be small to minimize changes in the B_m coil circuit and adding new perturbations to the system. While the $\Delta\omega$ we used are presented below, the specific choice of $\Delta\omega$ depends on the specifics of each application. For example, as $\Delta\omega$ decreases, separation of the two NMR peaks becomes less accurate and hence related measurements (e.g., relaxation time or spatial location in gradients) suffers similarly. Increasing $\Delta\omega$ will result in less effective transient removal. These competing factors must be balanced appropriately for each application.

Finally we point out that another variation of this approach is to change the direction of the measurement field during the data acquisition

$$\mathbf{B}_k = (-1)^k \mathbf{B}_0, \quad k = \overline{1,2n},$$

and selecting the polarization field (and consequently the initial magnetization of the sample) orthogonal to the normal of the pick-up coil, thus assuring that

$$F_k(t) = \int F_0(\omega') \sin((-1)^k \omega' t)\, d\omega' \equiv (-1)^k F_0(t).$$

In this approach the mean difference between odd and even measurements immediately yields the "typical" single-frequency FID.

3. Instrumentation

The data presented here were acquired using a system illustrated schematically in Fig. 1. The system uses a single low-T_c SQUID (Superconducting QUantum Interference Device [21]) coupled to the second order axial superconducting gradiometer (25 mm diameter and 40 mm baseline)

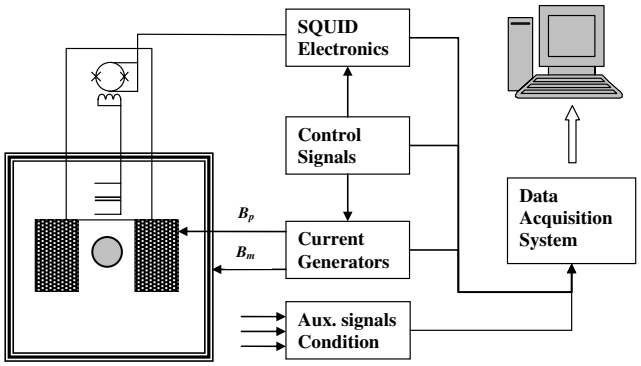

Fig. 1. Schematic diagram of the ULF NMR system. Current generators provide current to the magnetic field coils producing B_p and B_m. Control signals synchronize fields, the SQUID, and data acquisition. Auxiliary signals are also acquired during the experiment (for example sample temperature, etc.).

[22]. The balance level is better than 0.1% and the field resolution is about 3 fT/$\sqrt{\text{Hz}}$ that corresponds to the output voltage noise 15 μV/$\sqrt{\text{Hz}}$. The sample was pre-polarized in a magnetic field, B_p of up to 50 mT. The measurement field, B_m, was about 3 orders of magnitude smaller, <100 μT. Operation at magnetic fields comparable to or less than the earth's magnetic field was achieved by acquiring data inside a two layer magnetically shielded room [23]. B_p was generated by a pair of coils positioned orthogonal to the cryostat tail, and the sample was placed between them. The coils were constructed with Litz (multistranded) wire to minimize the thermal Jonson noise from the coils [24]. Each coil consisted of ~300 turns and the following dimensions: OD ~ 220 mm, ID ~ 110 mm, and thickness ~55 mm. The coils were separated by 62 mm. The inductance of the each coil was 8.7 mH; with a resistance of 0.46 Ω each. B_m was generated orthogonally to B_p by a rectangular Helmholtz coil pair. Each coil consists of ~100 turns with ~0.6 m sides. The inductance of the each coil was 100 mH; and a resistance of 15 Ω each.

Samples were pre-polarized in B_p for a time $>T_1$ of the sample while the SQUID electronics were effectively turned off. The experimental epoch was said to start at time $t = 0$, after which B_p was switched off at some time later depending on experimental requirements. Following the shutdown of B_p, the SQUID electronics were activated, and the precession signal about B_m was measured. The "dead time" associated with SQUID recovery and transients, the latter depending on the magnitude of B_p, was observed to be ~0.5 ms. At the end of a pre-defined measurement epoch time, the SQUID electronics were again de-activated, B_p switched back on, and the process repeated to acquire the next epoch. The measurement field was presented alternately: odd epochs—B_m, even epochs—$B'_m = B_m - \Delta B_m$. The typical change in the measurement field ΔB_m was 3.70 ± 0.01 μT, which corresponds to the Larmor frequency shift for protons 157.5 ± 0.4 Hz, however in the experiments with gaseous samples ΔB_m was 3.81 ± 0.01 μT (the Larmor frequency shift for protons 162.2 ± 0.4 Hz) due to slight modification of the measurement field circuit.

4. Results

We have tested our technique, described above, on a number of samples including distilled water, various $CuSO_4$ solutions (up to 0.5 M $CuSO_4$ in water), butane, and gaseous SF_6.

The NMR data recorded for a 2 ml sample of distilled water is plotted in the Fig. 2. The polarization time in this experiment was 0.25 s mainly to test the system's operation at the high repetition rate. Also the short polarization time ensured that the magnitude of the free induction decay signal is comparable with the one of gaseous samples. The upper panel on the Fig. 2 shows the averaged signals (175 trials) for two different frequencies (blue and green traces), and the difference (red trace) with DC offset removed. The difference signal is expanded in the center panel, and the Fourier spectrum of the difference is shown in the bottom panel. It is clearly evident in this figure that the transient signal is reduced by more than a factor of 10^4 (80 dB), while the remaining signal shows the typical "beat" characteristic of a signal containing two frequencies. Two peaks at 3037.86 ± 0.01 and 3195.04 ± 0.01 Hz are well resolved using the Fourier transform. Note that the width of the peaks and side lobes are associated with the signal duration (~120 ms). The difference in the frequency between these peaks is about 157.19 ± 0.01 Hz which corresponds to ΔB_m (the exact value of the frequency shift was measured independently using relatively big sample ~120 ml).

To test performance of our technique for measuring weak NMR signals and estimating parameters of weak FID signals with short relaxation times we used a 0.5 M $CuSO_4$ solution. The T_2^* time of the $CuSO_4$ solution was first measured using a single-frequency technique for a relatively large sample (~120 ml). Due to large amplitude of the FID signal relative to the transient-induced signal, it was possible to approximate and remove the transients using the exponential approximation described above (see, Eq. (1)). While the residual transient-induced signals were much smaller than the FID signal, we could not accurately fit a relaxation time to the FID. We estimated the relaxation time to be T_2^* approximately 1.5 ms with a very poor $\chi^2 > 25$. We were able to improve the χ^2 only after removing the first 1ms of the acquired FID that contained transients the exponentials could not fit. Removing the first 1ms of the FID and fitting the remaining transients with the exponentials enabled us to accurately estimate the T_2^* relaxation time to be 1.73 ± 0.01 ms with $\chi^2 \approx 1.2$.

Fig. 3 shows the NMR signal recorded for a 2 ml sample of the $CuSO_4$ solution obtained using a two frequency measurements and differencing the average signals of the two frequencies (~1000 averages for each frequency). In addition a 1000–5000 Hz bandpass filter was applied. We measured the width of the peaks at half height to be

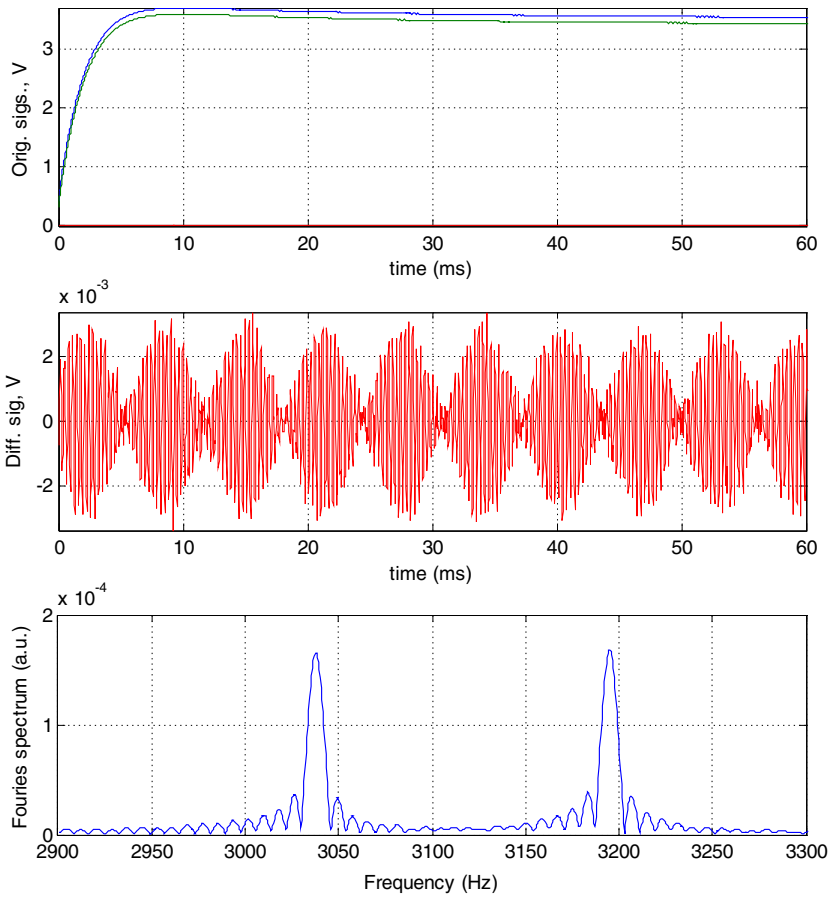

Fig. 2. (Top panel) measured signals with the two different frequencies (blue and green traces), and the difference between these signals with DC term removed (red trace), (middle panel) the difference plotted on an appropriate scale; (bottom panel) Fourier spectrum of the difference.

$\Delta f_{1/2} = 1/(\pi T_2^*) = 187$ Hz which more than the difference between the frequencies ~157 Hz. It should be noted that, the modulus of the difference of two complex Lorentz lines with the same amplitudes and damping factors is a unimodal function of frequency (i.e., a single peak with no "dip" between) when the difference between the central frequencies of these lines is less or equal then $\Delta f_{1/2}$. To resolve the frequency content of the FID signal and estimate the relaxation time we used typical time domain algorithms. We first applied the DECRA algorithm to obtain the initial estimation of number of harmonic components, frequencies, amplitudes and relaxation times (see Eq. (3)), and then refined the estimation of the harmonic components' parameters using discrete exponential fitting (DEF) technique [20]. We were able to resolve the FID into two harmonic components with frequencies 3037 ± 5 and 3193 ± 5 Hz and with the T_2^* relaxation time of 1.7 ± 0.2 ms for both components. The frequency shift between these components equals 156 ± 6 Hz.

We successfully applied this technique to record NMR signals and estimate relaxation times of samples of gaseous sulfur hexafluoride (SF_6). The samples were pure SF_6 gas with $\sim 4 \times 10^{19}$ molecules per cm^3 density at room temperature. The measurements were conducted for 20 and 60 cm^3 volumes. When we attempted to approximate the transients with exponentials, the residuals were much larger than the FID, hence we could obtain no meaningful results from this approach. Furthermore, spatial sensitivity distribution of the SQUID pickups prevented larger samples from being used to increase the signal.

Fig. 4 shows the NMR signals recorded for these samples using the two frequency technique. To improve signal-to-noise ratio for the Fourier spectra (shown on the bottom panel of the Fig. 4) we used additional apodization of the measured FID with the exponential function: $\exp(-(t/\tau)^2)$, where the parameter τ was 2.5 ms. It should be noted that the apodization, while improving visual representation of the spectra; also affects estimation of the relaxation times.

We used a water phantom to calibrate the ULF-NMR system immediately prior to measuring the SF_6 samples. The measured proton Larmor frequencies were: $F_1 = 3131.70 \pm 0.01$ and $F_2 = 3293.88 \pm 0.01$ Hz ($\Delta F = 162.18 \pm 0.01$ Hz). The expected Larmor frequencies for fluorine spins (based on the proton values) were: $F_1 = 2947.82 \pm 0.01$, $F_2 = 3100.48 \pm 0.01$, $\Delta F = 152.66 \pm 0.01$ Hz.

Direct application of the DECRA, DEF, or Lorentzian fit techniques to estimate the T_2^* relaxation time for the measurement we have presented does not result in robust

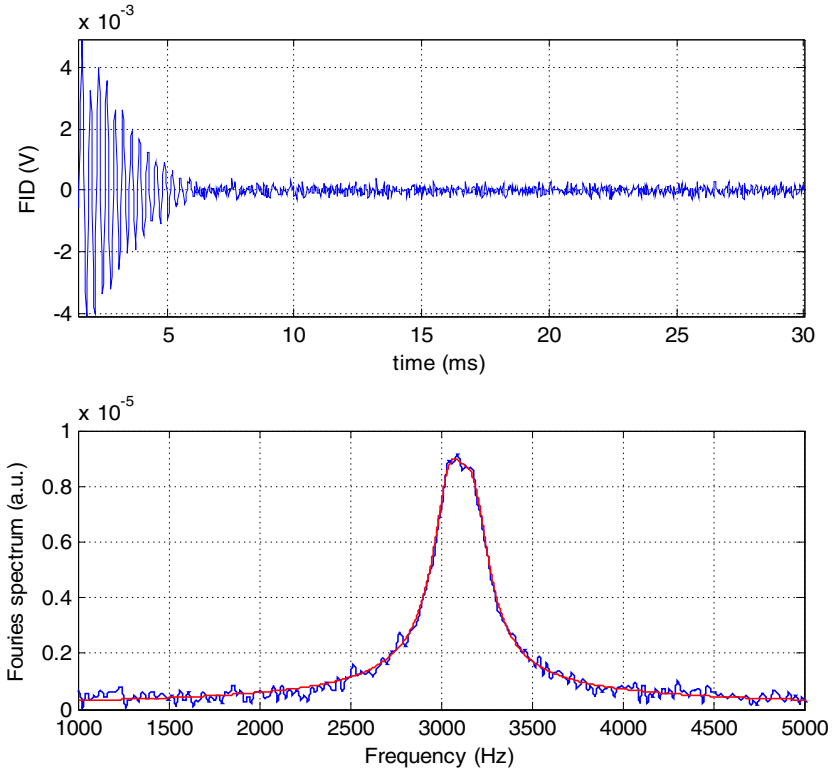

Fig. 3. (Top panel) two frequency FID of a 2 ml sample of water doped with copper sulfate; (bottom panel) Fourier spectrum of the FID (blue trace) and Lorentz line approximation (red trace), parameters of the approximation are found using the DECRA + DEF technique in the time domain.

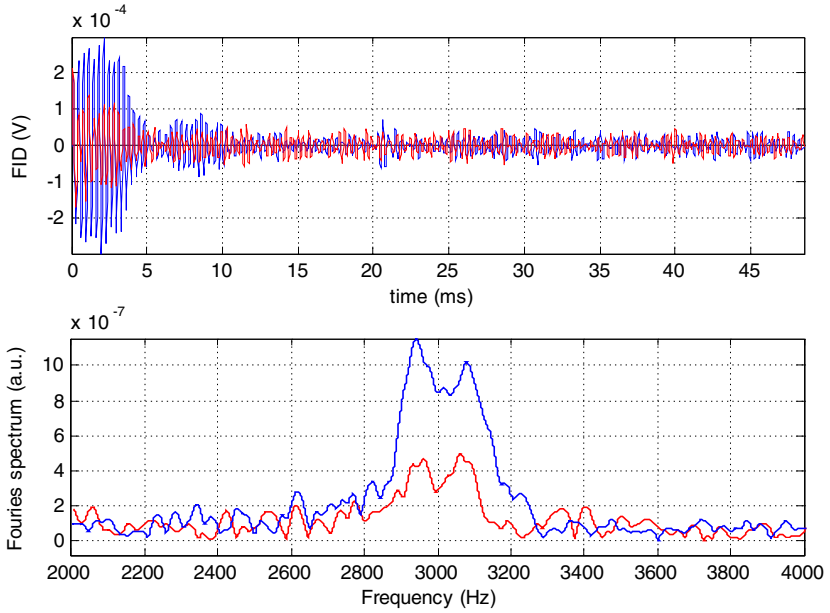

Fig. 4. (Top panel) two frequencies FID for SF_6 gas, red trace 20 cm^3 sample ($\sim 4.6 \times 10^{21}$ fluorine atoms), blue trace 60 cm^3 sample ($\sim 1.4 \times 10^{22}$ fluorine atoms); (bottom panel) the corresponding Fourier spectra. 10,000 averages.

solutions because of the low signal-to-noise. For example, we applied the DEF algorithm to data obtained for a large sample. The resulting estimation of the T_2^* time for the two components was 3 ± 1 and 4 ± 1 ms, with the frequency shift between these components $\Delta F = 167 \pm 9$ Hz. Estimating these values from ULF-NMR data acquired for a small sample was even worse. We achieved some improvement by applying the Cadzow algorithm (iterative signal enhancement algorithm based on a singular value decomposition (SVD) of the Hankel matrix constructed

from a single FID) [25,26], however the results remain very sensitive to the specifics of the applied algorithms.

We significantly improved the estimation of the relaxation times by applying the conditions defined in Eq. (4) as an *a priori* condition. Using this approach, we estimated T_2^* relaxation time of SF_6 gas to be 4.2 ± 0.3 ms for the large sample and 4 ± 1 ms for the small sample. This example shows that the estimation of the relaxation times became significantly more robust, that is the uncertainty in estimation of the T_2^* relaxation time is reduced by more than a factor of 3, with the use of the above conditions.

Our results may be compared with the earlier results obtained at high fields. According to [27] the ratio of ^{19}F T_1 relaxation time to the density of the sample in amagat numbers for pure SF6 measured at 4.7 T (188 MHz) and 300 K is 2.13 ± 0.02 ms amagat^{-1} (one amagat is 2.687×10^{19} molecules per cm^3). It should be noted that the experiments of both the cited work and this work are in the extreme narrowing limit [28], where T_1 and T_2 are equal. Taking into account the density of the samples in our experiments ($\sim$1.5 amagat) the equivalent T_2 time is 3.20 ± 0.03 ms compared to our measured value of 4.2 ± 0.3 ms. Since ours were proof of principle experiments, little attention was paid to accurately determining the sample temperature and density which likely contributes to the descripancy between the two values.

5. Discussion and conclusion

There is a growing interest in NMR measurements at ULF spurred by several physics benefits and a large variety of novel applications realized at these low fields. We have pointed to the narrow NMR peak-width, virtual absence of susceptibility artifacts (particularly important in magnetic resonance imaging), and the ability to image materials inside metal containers, to name just a few. The typical approach of prepolarizing the sample prior to measuring the NMR signal results in large transient signals that interfere with the measurement. Furthermore, this transient signal is correlated with the measurement, hence is not reduced by typical averaging approaches.

The distortion is largely a consequence of eddy currents induced in any conducting material near the sample, including the magnetic field coils and the measurement system. These effects are particularly pronounced in the first few milliseconds of the measurement due to typical induced eddy current decay times. While NMR signals from samples with long T_1 times can readily be analyzed by removing (or not acquiring) the first few milliseconds of the FID, this approach is not feasible for samples with short T_1 times.

In this paper, we described a general approach that largely cancels the transient signals. While the technique is applicable to any sample, it is of most practical valuable for samples containing materials with T_1 in the range from $<$1 ms to $\sim$5 ms. We described a method by which the FID is acquired at two similar by different measurement fields, B_m. By differencing the two FID's, the correlated transient signal is eliminated while the FID's (which occur at two slightly different frequencies) are retained. Successive averaging of such data is used to remove uncorrelated noise.

We have applied this technique to demonstrate the first measurements of very short T_1 time materials at ultra-low field. We measured the NMR spectra of a variety of samples including 0.5 M $CuSO_4$ in water and gaseous SF_6 with T_1 times in the range of 1–4 ms. Our dual-frequency transient cancellation technique reduced the transient signal by four orders of magnitude ($\sim$80 dB) for typical samples and experimental conditions. This technique will be important for broad application of ULF-NMR by enabling the measurement of NMR signals from short T_1 time materials that would otherwise be impossible.

Acknowledgments

The authors acknowledge technical contributions made to this work by Vadim Zotev and Henrik Sandin. We also thank the US Department of Energy and the Los Alamos National Laboratory for their support.

References

[1] X. Hu, D.G. Norris, Advances in high-field magnetic resonance imaging, Annu. Rev. Biomed. Eng. 6 (2004) 157–184.
[2] A. Macovski, S. Conolly, Novel approaches to low cost MRI, Magn. Reson. Med. 30 (1993) 221–230.
[3] A.N. Matlachov, P.L. Volegov, M.A. Espy, J.S. George, R.H. Kraus Jr., SQUID detected NMR in microtesla magnetic fields, J. Magn. Reson. 170 (2004) 1–7.
[4] R. McDermott, A.H. Trabesinger, M. Mück, E.L. Hahn, A. Pines, J. Clarke, Liquid-state NMR and scalar couplings in microtesla magnetic fields, Science 295 (2002) 2247–2249.
[5] U.A. Ramadan, A.T. Markkola, J. Halavaara, J. Tanitu, A.M. Hakkinen, H.J. Aronen, On- and off resonance spin-lock MT imaging of normal human brain at 0.1 T: Possibilities to modify image contrast, Magn. Reson. Imaging 16 (1998) 1191–1199.
[6] N.Q. Fan, M.B. Heaney, J. Clarke, D. Newitt, L.L. Wald, E.L. Hahn, A. Bielecki, A. Pines, Nuclear magnetic resonance with DC SQUID preamplifiers, IEEE Trans. Magn. 25 (1989) 1193–1199.
[7] M.P. Augustine, D.M. TonThat, J. Clarke, SQUID detected NMR and NQR, Solid State Nucl. Magn. Reson. 11 (1998) 139–156.
[8] K. Schlenga, R.F. McDermott, J. Clarke, R.E. de Souza, A. Wong-Foy, A. Pines, Low-field magnetic resonance imaging with a High-Tc dc superconducting quantum interference device, Appl. Phys. Lett. 75 (1999) 3695–3697.
[9] H.C. Seton, J.M.S. Hutchison, D.M. Busell, A 4.2 K receiver coil and SQUID amplifier used to improve SNR of low-field magnetic resonance images of the human arm, Meas. Sci. Technol. 8 (1997) 198–207.
[10] S. Kumar, W.F. Avrin, B.R. Whitecotton, NMR of room temperature samples with a flux-locked dc SQUID, IEEE Trans. Magn. 32 (1996) 5261–5264.
[11] R. McDermott et al., SQUID-detected magnetic resonance imaging in microtesla magnetic fields, J. Low Temp. Phys. 135 (2004) 793–821.
[12] M.A. Espy, A.N. Matlachov, P.L. Volegov, J.C. Mosher, R.H. Kraus Jr., SQUID-based simultaneous detection of NMR and biomagnetic signals at ultra-low magnetic fields, IEEE Trans. Appl Superconduct. 15 (2) (2005) 635–639.

[13] A. Abragam, Principles of Nuclear Magnetism, Oxford University Press, Oxford, 1961.
[14] M. Packard, R. Varian, Free nuclear induction in the Earth's magnetic field, Phys. Rev. 93 (1954) 941.
[15] A. Bloom, D. Mansir, Measurement of nuclear induction relaxation times in weak magnetic fields, Phys. Rev. 93 (1954) 941.
[16] A.N. Matlachov, P.L. Volegov, et al., Instrumentation for simultaneous detection of low field NMR and biomagnetic signals, IEEE Trans. Appl. Superconduct. 15 (2) (2005) 676–679.
[17] P. Volegov, A.N. Matlachov, M.A. Espy, J.S. George, R.H. Kraus Jr., Simultaneous magnetoencephalography and SQUID detected nuclear MR in microtesla magnetic fields, Magn. Reson. Med. 52 (2004) 467–470.
[18] A. Nordon, P.J. Gemperline, C.A. McGill, D. Littlejohn, Quantitative analysis of low-field NMR signals in the time domain, Anal. Chem. 73 (2001) 4286–4294.
[19] Guang Zhu, Yingbo Hua, Quantitative NMR signal analysis by an iterative quadratic maximum likelihood method, Chem. Phys. Lett. 264 (1997) 424–428.
[20] Henrik Toft Pedersen, Rasmus Bro, Søren Balling Ehgelsen, Towards rapid and unique curve resolution of low-field NMR relaxation data: Triliniar SLICING versus two-dimensional curve fitting, J. Magn. Reson. 157 (2002) 141–155.
[21] J. Clarke, SQUID Fundamentals, in: H. Weinstock (Ed.), SQUID Sensors: Fundamentals, Fabrication and Aplications, NATO ASI Series, E329, Kluwer Academic Publishers, 1996, pp. 1–62.
[22] J. Vrba, SQUID Gradiometers in Real Environment, in: H. Weinstock (Ed.), SQUID Sensors: Fundamentals, Fabrication and Aplications, NATO ASI Series, E329, Kluwer Academic Publishers, 1996, pp. 117–178.
[23] IMEDCO, http://www.imedco-shielding.com.
[24] Michael Mößle, Whittier R. Myers, Seung-Kyung Lee, Nathan Kelso, Michael Hatridge, Alexander Pines, John Clarke, SQUID-detected in vivo MRI at microtesla magnetic fields, IEEE Trans. Appl. Superconduct. 15 (2) (2005) 757–760.
[25] Ulrich Günther, EuroLabCourse Advanced Computing in NMR Spectroscopy, Florence, Sept. 2001.
[26] J. Cadzow, Signal Enhancement. A Composite Property Mapping Algorithm, IEEE Trans. Acoustics, Speech, and Signal Processing, ASSP-36 (1988) pp. 49–62.
[27] J. Cynthia, A. Jameson, Keith Jameson, Effective collision cross sections for SF6 from nuclear magnetic relaxation, J. Chem. Phys. 88 (12) (1988) 7448–7452.
[28] J.A. Courtney, R.L. Armstrong, A nuclear spin relaxation study of the spin-rotational interactions in spherical top molecules, Canadian J. Phys. 50 (12) (1972) 1252–1261.